JACS
JOURNAL OF THE AMERICAN CHEMICAL SOCIETY

pubs.acs.org/JACS

Article

Surface-Templated Glycopolymer Nanopatterns Transferred to Hydrogels for Designed Multivalent Carbohydrate–Lectin Interactions across Length Scales

Anamika Singh, Juan C. Arango, Anni Shi, Joseph B. d'Aliberti, and Shelley A. Claridge*

Cite This: *J. Am. Chem. Soc.* 2023, 145, 1668–1677

Read Online

ACCESS | Metrics & More | Article Recommendations | Supporting Information

ABSTRACT: Multivalent interactions between carbohydrates and proteins enable a broad range of selective chemical processes of critical biological importance. Such interactions can extend from the macromolecular scale (1–10 nm) up to much larger scales across a cell or tissue, placing substantial demands on chemically patterned materials aiming to leverage similar interactions in vitro. Here, we show that diyne amphiphiles with carbohydrate headgroups can be assembled on highly oriented pyrolytic graphite (HOPG) to generate nanometer-resolution carbohydrate patterns, with individual linear carbohydrate assemblies up to nearly 1 μm, and microscale geometric patterns. These are then photopolymerized and covalently transferred to the surfaces of hydrogels. This strategy suspends carbohydrate patterns on a relatively rigid polydiacetylene (persistence length ~ 16 nm), exposed at the top surface of the hydrogel above the bulk pore structure. Transferred patterns of appropriate carbohydrates (e.g., *N*-acetyl-D-glucosamine, GlcNAc) enable selective, multivalent interactions (K_D ~ 40 nM) with wheat germ agglutinin (WGA), a model lectin that exhibits multivalent binding with appropriately spaced GlcNAc moieties. WGA binding affinity can be further improved (K_D ~ 10 nM) using diacetylenes that shift the polymer backbone closer to the displayed carbohydrate, suggesting that this strategy can be used to modulate carbohydrate presentation at interfaces. Conversely, GlcNAc-patterned surfaces do not induce specific binding of concanavalin A, and surfaces patterned with glucuronic acid, or with simple carboxylic acid or hydroxyl groups, do not induce WGA binding. More broadly, this approach may have utility in designing synthetic glycan–mimetic interfaces with features from molecular to mesoscopic scales, including soft scaffolds for cells.

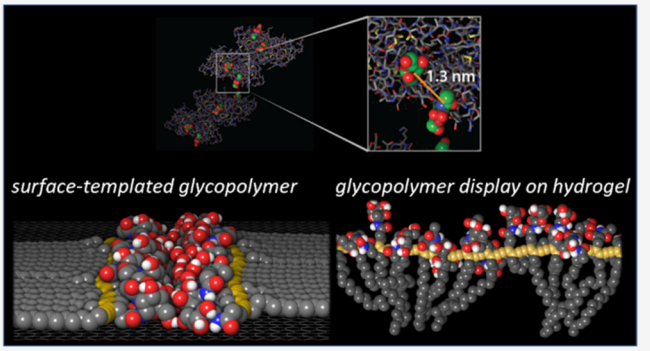

INTRODUCTION

All living cells are decorated by a dense, complex array of glycans—oligo- and larger polysaccharides that are expressed on cell surfaces in various forms (e.g., free oligosaccharides, glycoproteins, and glycolipids). Cell surface glycans are recognized by glycan binding proteins, also referred to as lectins.[1,2] Lectins have been known in plants since the 1880s, but over time, it has also become clear that glycan–lectin interactions mediate or modulate a wide range of cellular interactions in animals as well (e.g., cell–cell adhesion, intracellular routing of glycoproteins, differentiation and tumor metastasis, and viral infections).[2,3]

Understanding and controlling glycan–lectin interactions at the molecular level is central to the development of diagnostic and therapeutic tools,[4−10] engineering new carbohydrate-binding proteins,[11,12] and design of materials to scaffold cell growth for regenerative medicine.[13] One challenge in replicating glycan–lectin interactions occurring in vivo is the relatively weak binding (dissociation constant, K_D, in the mM range) between individual carbohydrates and lectins.[14] Biological systems have evolved to take advantage of this weak interaction, creating selectivity for specific glycans by incorporating multiple receptors in each lectin, shifting K_D from the mM to the nM range.

Designing materials that utilize carbohydrate–lectin interactions requires detailed control over placement and orientation of carbohydrates over scales from 1 to 10 nm for individual lectins and up to 100 nm or more when lectins themselves are clustered, as in a viral capsid.[5,15] For instance, the wheat germ agglutinin (WGA) protein exhibits binding specificity for *N*-acetyl-D-glucosamine (GlcNAc) and *N*-acetyl-D-neuraminic acid (sialic acid, Sia), with a 1.3 nm distance between receptor sites for GlcNAc (Figure 1a)[14] and 3.9 nm for Sia,[16] while concanavalin A (ConA) has a distance of ~6.5 nm between mannose binding sites.[17] Carbohydrate linkage

Received: September 17, 2022
Published: January 14, 2023

https://doi.org/10.1021/jacs.2c09937
J. Am. Chem. Soc. 2023, 145, 1668–1677

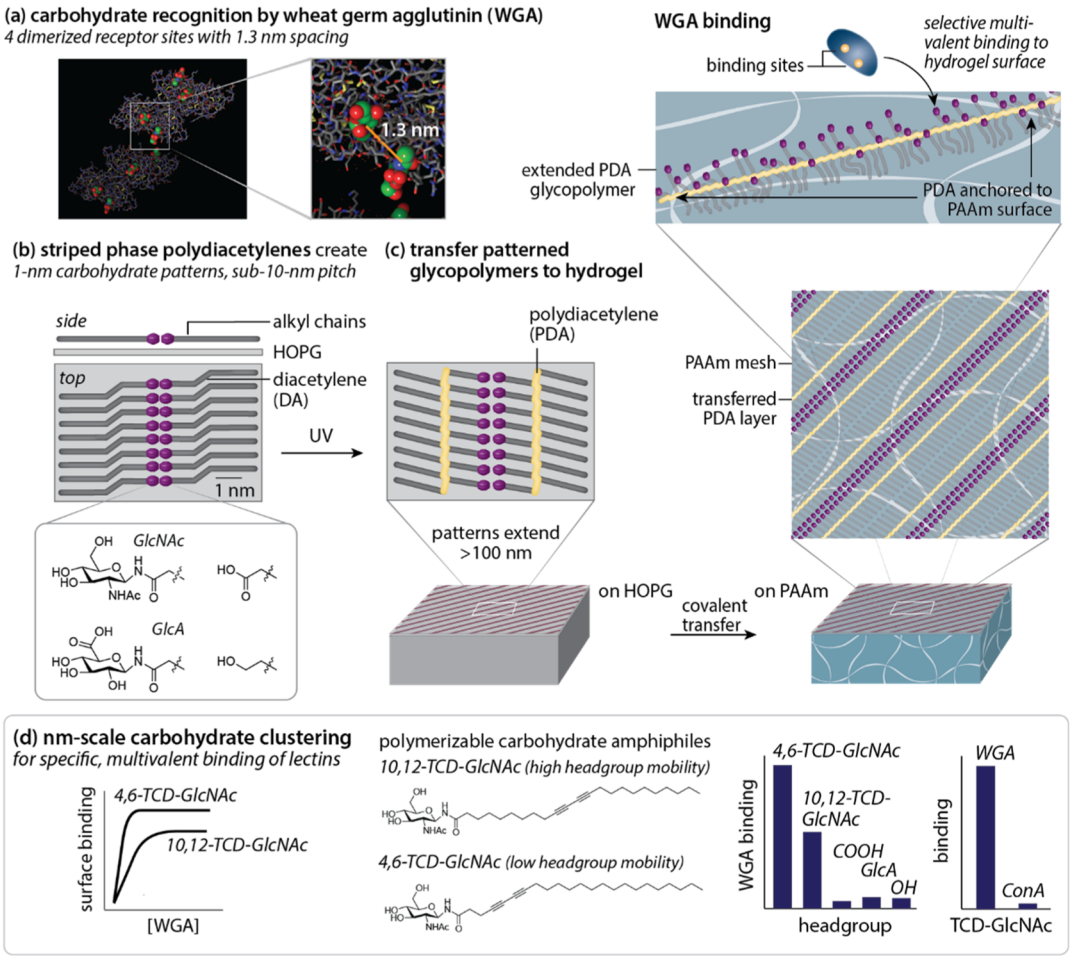

Figure 1. (a) Schematic illustrating multivalent GlcNAc recognition by WGA (PDB: 2UVO). (b) Schematic of striped phase assembly and structure on HOPG. (c) Schematic of PDA transfer to PAAm, in relation to PAAm polymerization architecture, and extended glycopolymer display for selective multivalent binding. (d) Illustration of binding selectivity for WGA at striped interfaces based on the choice of carbohydrate amphiphile used for striped phase assembly. Parts of panel (b) adapted with permission from ref 56. Copyright 2022 American Chemical Society.

and ring orientation are also important factors[18] (e.g., α2,3-linked Sia is associated with avian influenza viruses and α2,6-linkages with human viruses[19]). Such interactions can also span larger scales when lectins are clustered for recognition. For example, the diameter of a typical hemagglutinin lectin expressed on the influenza A virus (IAV) surface is ca. 14 nm, while the virus diameter is 100−150 nm;[20] the targeted glycan length is ca. 2−20 nm, with multiple glycans binding to lectins across the IAV surface.[21] More broadly, the distribution of glycans across a cell surface can lead to pattern formation over length scales from nanometers to micrometers,[22] extending to even larger scales across tissues.

Materials designed for carbohydrate display have become increasingly important over the past two decades, as the breadth of function of the glycocalyx has become more broadly appreciated. Glycopolymers based on a number of scaffolds (e.g., linear synthetic polymers,[17] dendrimers,[23] other branched oligomers,[24] peptides,[25] and proteins[26]) have been shown to provide aspects of control over carbohydrate display, including valency, nanometer-scale binding group spacing, and architecture.[17,27]

Monosaccharides and glycans may also be displayed at interfaces, providing convenient readouts of binding interactions as well as the potential for longer-range ensemble interactions. Glycan microarrays have been designed to screen glycan−lectin interactions,[15,26,28−33] with functionalized monosaccharides, glycans, or glycopolymers typically derivatizing solid surfaces such as glass, silicon, and gold over microscopic areas.[28,34] More recently, there have been growing efforts to design synthetic glycocalyx mimics that recreate specific glycan functions in more biological environments including cell membranes,[35,36] softer interfaces that reveal the importance of surface curvature, mechanical coupling, and dynamics, among other factors.[5]

In designing glycomaterials for interactions with biological systems, it is also important to consider routes for controlling interfaces of soft synthetic materials such as those used in implantation. Here, we report an unconventional and potentially broadly applicable route to control glycan display from molecular to microscopic scales, on both hard and soft substrates, combining desirable aspects of polymer and surface-based approaches to bridge length scales. Our approach is based on lying-down phases of diacetylene (DA) amphiphiles,[37−41] which assemble with the amphiphile alkyl chains parallel to the HOPG surface (Figure 1b), creating 1 nm wide stripes of polar headgroups with a tunable pitch (5−10 nm) based on alkyl chain length.[42] Individual molecular rows can extend to lengths >10 μm, depending on molecular architecture.[46] Topochemical photopolymerization of the DAs generates stripes of conjugated polydiacetylenes

https://doi.org/10.1021/jacs.2c09937
J. Am. Chem. Soc. 2023, 145, 1668−1677

(sPDAs) that link functional headgroups[43] along the relatively rigid PDA backbone (persistence length ~ 15 nm),[44,45] with an alkyl segment of controlled length between the PDA and the patterned functionality. Previously, using simple functional headgroups (e.g., COOH, NH_2), we have demonstrated that patterning can be controlled over large areas (several cm^2, with individual molecular domains $>10^4$ μm^2 for some molecules).[46−48] We have also used microcontact printing to achieve geometric control over positioning of nanoscale pattern elements over microscopic areas suitable for controlling interactions with cells and other biological entities.[48−51] Hierarchical surface patterns generated in this way influence both interfacial wetting[41,52,53] and further assembly at the interface.[51,54,55] Recently, we have shown that sPDAs on HOPG can be utilized in a reaction process that transfers the nanometer-resolution functional patterns to soft, biocompatible substrates (Figure 1c) such as polydimethylsiloxane (PDMS)[49−51] and polyacrylamide (PAAm) hydrogels.[56] Functional patterns are suspended above the porous gel structure, enhancing steric accessibility.

Building on this powerful chemical patterning approach, here we synthesize polymerizable amphiphiles with carbohydrate headgroups [e.g., *N*-acetyl-D-glucosamine (GlcNAc) and glucuronic acid (GlcA)], using sPDA assembly as a means to achieve nanometer-resolution carbohydrate patterning that mimics key aspects of glycan architectures, including molecular (1−10 nm) and mesoscale (>100 nm) structures. We further demonstrate that these carbohydrate patterns can be transferred to the surface of PAAm hydrogels, allowing for binding interactions to be screened under mechanical conditions more analogous to those in vivo, in comparison with patterns on hard materials such as glass and gold. Finally, we show that GlcNAc sPDAs generate highly selective interactions with WGA and that modifying the amphiphile structure to increase local GlcNAc concentration also increases binding avidity. Together, these findings suggest the utility of this surface-templated glycopolymer architecture in designing multivalent glycan−protein interactions for cell scaffold materials or other applications such as understanding mechanical contributions to multivalent glycan interactions.

RESULTS AND DISCUSSION

Synthesis of Amphiphiles. To test for WGA binding selectivity, amphiphiles with GlcNAc and GlcA headgroups, as well as OH and COOH functional groups common in glycans, were prepared (Scheme 1a) through modifications of previously reported procedures.[57] Additionally, to examine the role of the alkyl chain segment proximal to the headgroup in spatially constraining carbohydrates for multivalent binding, two isomeric GlcNAc amphiphiles (10,12-TCD-GlcNAc and 4,6-TCD-GlcNAc) were synthesized. 4,6-TCD-GlcNAc positions the diyne much closer to the carbohydrate headgroup, potentially resulting in tighter ligand clustering, which would be predicted to decrease K_D.

To generate the polymerizable glycan amphiphiles, first, 4,6-tricosadiynoic acid (4,6-TCD-COOH) was synthesized by Cadiot−Chodkiewicz coupling (see detailed Experimental Methods in the Supporting Information). To generate amphiphiles with GlcNAc-modified headgroups, 4,6-TCD-COOH and 10,12-TCD-COOH (commercially available) were treated with oxalyl chloride [$(COCl)_2$] in the presence of catalytic amounts of DMF to obtain 4,6-TCD-COCl and 10,12-TCD-COCl, respectively (Scheme 1b). This process

Scheme 1. Structures and Syntheses of Diyne Amphiphiles

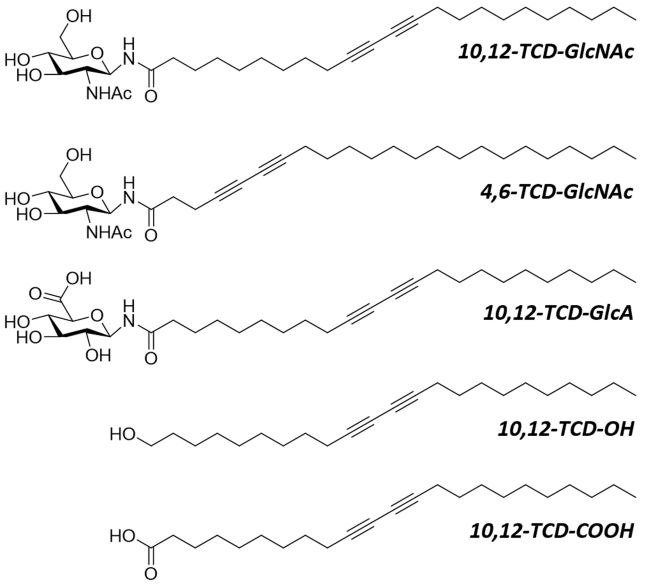

activates the carbonyl group toward nucleophilic substitution. Conjugation of GlcNAc to the diynoyl chloride (e.g., TCD-COCl) was performed using a trimethyl phosphine (PMe_3)-mediated Staudinger reaction (Scheme 1c). Finally, the *O*-acetyl protecting groups were removed from the conjugated intermediate by Zemplén deacetylation.

For simplicity, since all but one of the amphiphiles has the 10,12-TCD chain structure, we refer to these amphiphiles as TCD-GlcNAc, TCD-GlcA, TCD-OH, and TCD-COOH throughout the manuscript until the final section, in which the 4,6- and 10,12-TCD-GlcNAc isomers are compared.

Assembly of sPDA Monolayers on HOPG. Patterns of amphiphiles with carbohydrates or other functional headgroups were prepared by generating monolayers of diyne amphiphiles (e.g., TCD-GlcNAc) on HOPG (Figure 2a, left) through Langmuir−Schaefer (LS) conversion (see Experimental Methods in the Supporting Information). Briefly, this approach begins by ordering molecules as a standing phase Langmuir film on an aqueous subphase; a heated HOPG substrate is then lowered horizontally into contact with the Langmuir film, causing a subset of the molecules to reorder from the standing phase on water into a lamellar (striped) phase on the HOPG substrate. For TCD-GlcNAc, this arrangement forms a lamellar structure centered on ~1.7 nm

https://doi.org/10.1021/jacs.2c09937
J. Am. Chem. Soc. 2023, 145, 1668−1677

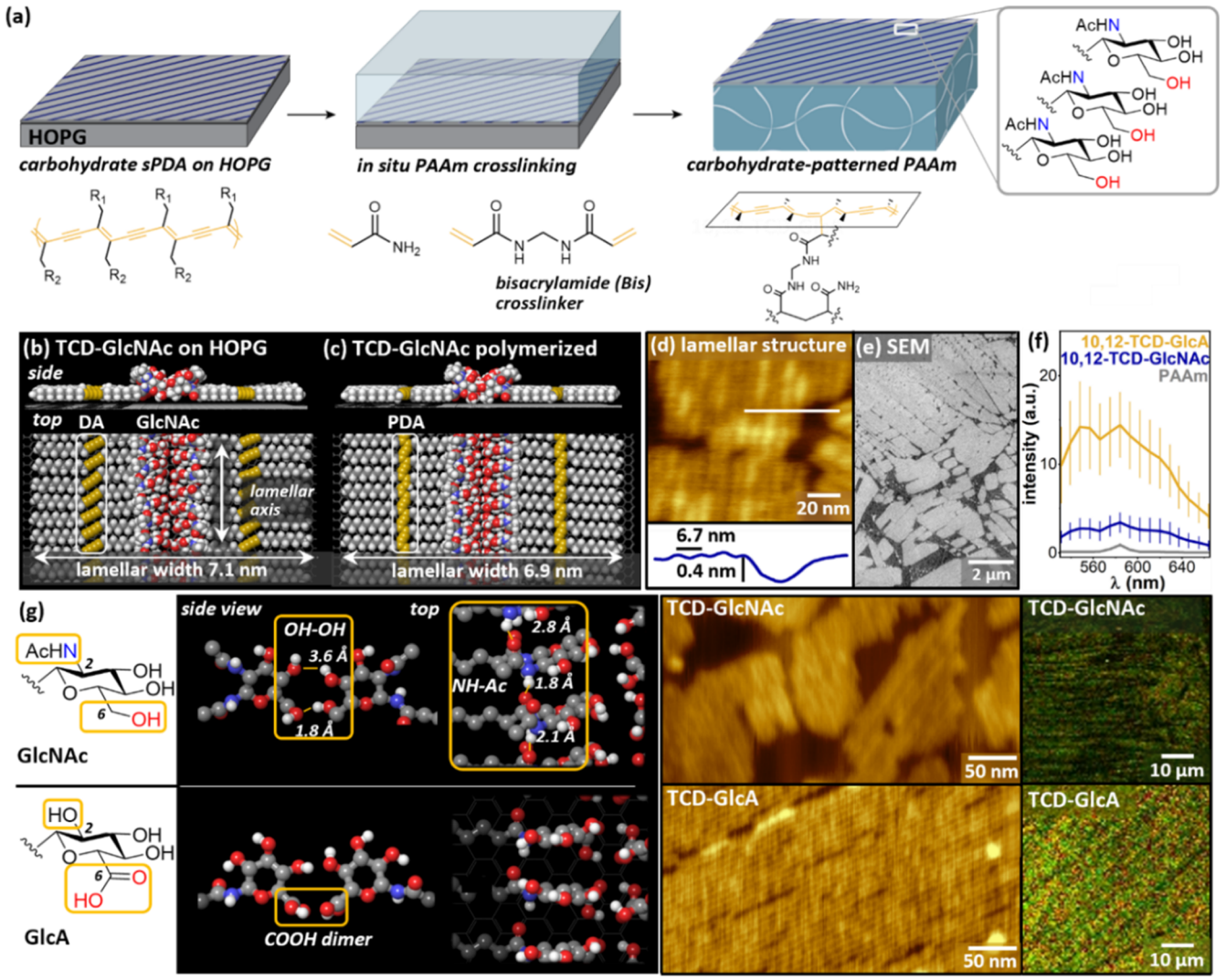

Figure 2. (a) Schematic of the carbohydrate sPDA pattern transfer to PAAm. (b,c) Molecular models of (b) unpolymerized and (c) polymerized TCD-GlcNAc monolayers on HOPG. (d) AFM images illustrating the lamellar structure of the polymerized TCD-GlcNAc monolayer. (e) SEM image illustrating the presence of microscale domain structure. (f) Fluorescence spectra of TCD-GlcNAc and TCD-GlcA on PAAm. (g) Chemical structures of GlcNAc and GlcA (left panel) and molecular models illustrating headgroup interactions in striped phases of TCD-GlcNAc and TCD-GlcA on HOPG (left center panel). AFM micrographs of TCD-GlcNAc and TCD-GlcA on HOPG (right center panel). Fluorescence micrographs of TCD-GlcNAc and TCD-GlcA on PAAm (right panel). Parts of panel (a) adapted from ref 56 with permission. Copyright 2022 American Chemical Society.

wide stripes comprising two opposing rows of GlcNAc, with alkyl chains on both edges, ca. 7 nm in width (Figure 2b,c). In AFM images (Figure 2d), the measured lamellar periodicity of 6.7 nm is in good agreement with the modeled structure (Figure 2c).[58] The size scale of molecular domains formed in this way can exceed length scales that are readily imaged by AFM; however, previously we have illustrated that SEM can be used to visualize long-range ordering of molecular domains,[59] as shown in Figure 2e.

Transfer of sPDA Monolayers from HOPG to Polyacrylamide. Next, we covalently transferred the surface-templated glycopolymers to PAAm, using a covalent transfer strategy (Figure 2a, center and right) in which PAAm is cured in contact with the carbohydrate sPDA on HOPG and then exfoliated. We have recently demonstrated that this process is effective in transferring sPDAs with simple headgroup chemistries (carboxylic acids or amines) to PDMS[49] or to PAAm.[56] Here, we take advantage of this approach to pattern more complex carbohydrate headgroup chemistries, in order to generate selective multivalent binding on the amorphous hydrogel surface. See the Supporting Information for a more detailed discussion of the transfer process, including cryoEM images of functionalized and unfunctionalized gel surfaces, and characterization of the PAAm mesh structure.

To assess whether the functionalized PAAm surfaces yield specificity for carbohydrates known to bind WGA, we assembled and photopolymerized monolayers of TCD-GlcNAc and TCD-GlcA (Figure 2f,g). GlcNAc is known to bind to WGA, while GlcA does not.[14] GlcNAc and GlcA differ at two substituents on the pyranose ring (Figure 2g left): at C2, GlcNAc has a bulky acetamido (−NHAc) group, while GlcA has a smaller OH; at C6, GlcNAc has an OH group, and GlcA has a COOH group.

Minimized molecular models of the two sPDAs indicate that C6 is one of the pyranose ring positions that mediates

https://doi.org/10.1021/jacs.2c09937
J. Am. Chem. Soc. 2023, 145, 1668−1677

interactions between opposing rows of headgroups along the lamellar median, with GlcA forming strong H-bonded COOH dimers and GlcNAc forming weaker H-bonds between OH groups. Experimentally, we observed that TCD-GlcNAc forms smaller ordered molecular domains (typical domain sizes 200−300 nm, Figure 2g, top right) on HOPG in comparison with TCD-GlcA (700−900 nm, Figure 2g, bottom right) and other amphiphiles with simpler head groups (see the Supporting Information). This would be consistent with the weaker inter-OH H-bonding and possibly also the presence of the bulky acetamido group.

Following in situ PAAm curing and exfoliation, confocal spectroscopy and microscopy (Figure 2f,g, far right) illustrate surface morphological features and spectral emission features characteristic of sPDA transfer, including a primary emission peak centered at 548 nm and sidebands extending up to ∼640 nm. While the spectral characteristics for TCD-GlcNAc emission are similar to those we have observed previously for other sPDAs with simpler headgroup chemistries, emission intensity is somewhat lower, pointing to the possibility of lower transfer efficiency (discussed more extensively in the following section). TCD-GlcA transfers more efficiently, as evident based on greater emission intensity; this is potentially consistent with previous work in which we have shown that monolayer chemistries that produce longer sPDAs also result in more efficient transfer.[60] Transfer is also visible in cryoEM images (Figures S5−S7) as a smoothing of the surface gel pore structure, consistent with a very thin nanoscale surface layer that is more tightly cross-linked than the bulk gel structure. PDAs are known to exhibit a polarized excitonic ^1B_u transition, oriented along the polymer backbone.[61] Polarized fluorescence emission images (Figure S8) of amphiphiles that exhibit long-range order also exhibit anisotropic emission consistent with partial retention of PDA alignment, although presumably ordering is not as strict as that observed on the HOPG substrate. Given the relatively open PAAm gel mesh structure, we anticipate that this results at least in part from the additional cross-linking in the surface layer, visible in cryoEM.

Selectivity of WGA toward the TCD-GlcNAc Monolayer. To assess the selectivity of WGA interaction with TCD-GlcNAc monolayers, we functionalized PAAm with amphiphiles having headgroups representing individual functional groups common in glycans (Figure 3): a hydroxyl group (TCD-OH) and a carboxylic acid (TCD-COOH). Additionally, we functionalized PAAm substrates with sPDAs generated from a GlcA amphiphile (TCD-GlcA), with a carbohydrate headgroup that is not a target for WGA binding. The fluorescence-based assays described in this section and following sections are not possible on HOPG substrates, which quench fluorescence.[49]

We exposed sPDA-functionalized PAAm surfaces to rhodamine-labeled WGA (5 μg/mL). Greater emission intensity from TCD-GlcNAc-functionalized PAAm (Figure 3a) in comparison to other functionalized substrates (Figure 3b−d) exposed to WGA illustrates the preferential binding of WGA to TCD-GlcNAc. Interestingly, this increased binding occurs in spite of the relatively modest transfer efficiency of TCD-GlcNAc (Figure 3e) in comparison with the other surface chemistries (Figure 3f−h).

To control for differences in the level of surface functionalization, we quantified fluorescence emission from monolayers before (Figure 3i) and after WGA exposure (Figure 3j; note the larger intensity scale following WGA

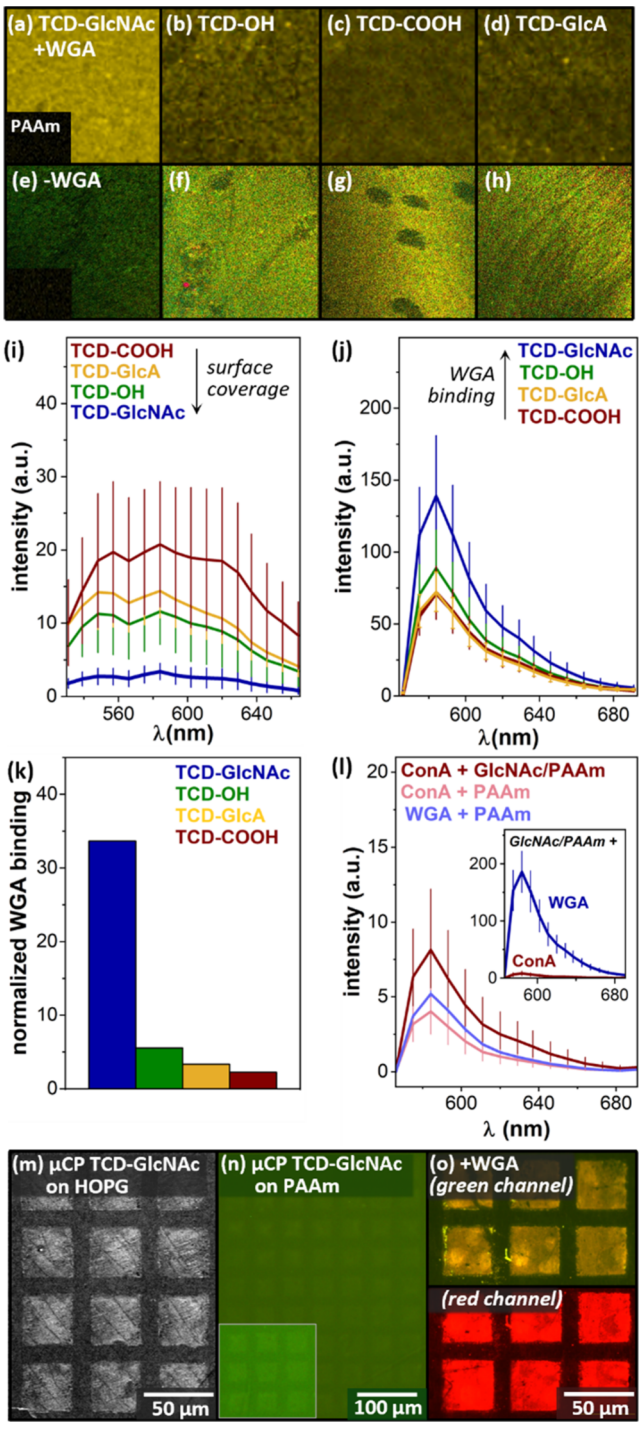

Figure 3. (a−d) Fluorescence images of monolayers after exposure to WGA (5 μg/mL). (e−h) Fluorescence images of monolayer on PAAm. (i,j) Fluorescence spectra of monolayers (i) before and (j) after exposure to WGA (5 μg/mL). (k) WGA binding to monolayers normalized for surface coverage. (l) Fluorescence spectra illustrating minimal increase in adsorption of rhodamine-labeled ConA (5 μg/mL) to TCD-GlcNAc/PAAm (red trace) vs unfunctionalized PAAm (light red). WGA exposed to unfunctionalized PAAm is shown for comparison (light blue). Higher gain settings were used in (l) to adequately resolve spectral differences at low emission intensity, leading to the higher observed fluorescence for the TCD-GlcNAc + WGA trace in comparison with the intensity in (j). (m−o) μCP patterned TCD-GlcNAc (m) on HOPG, (n) after transfer to PAAm, and (o) after transfer to PAAm and exposure to WGA. Inset in (n) uses enhanced contrast to emphasize square pattern.

https://doi.org/10.1021/jacs.2c09937
J. Am. Chem. Soc. 2023, 145, 1668−1677

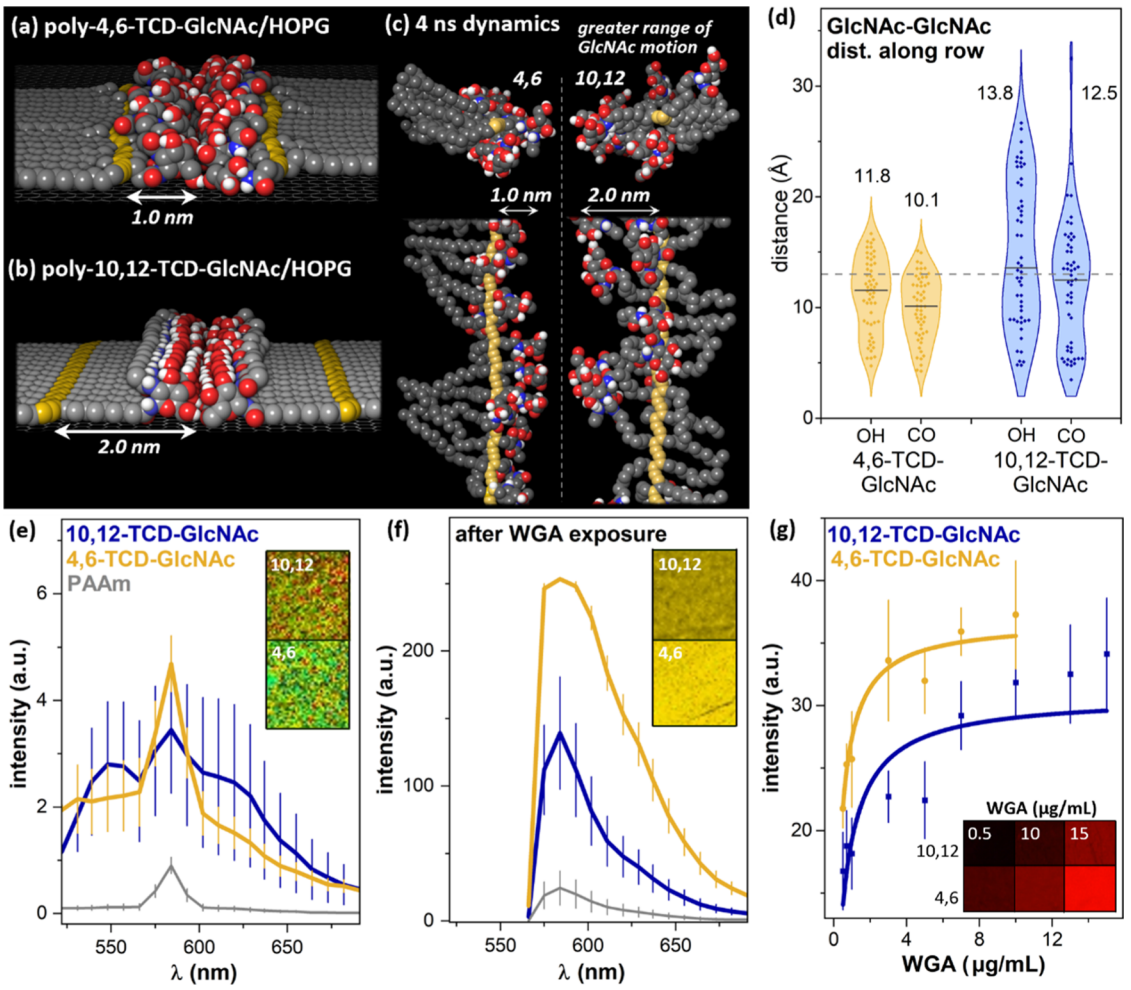

Figure 4. (a,b) Molecular models and dynamics of headgroup regions in polymerized monolayers of (a) 4,6-TCD-GlcNAc/HOPG and (b) 10,12-TCD-GlcNAc/HOPG. (c) Models following 4 ns dynamics with HOPG removed and PDA frozen, to simulate conditions on sPDAs transferred to PAAm. (d) Distribution of neighboring GlcNAc−GlcNAc distances along each sPDA. Gray tie line at 13.0 Å represents the distance between dimerized WGA binding sites. (e,f) Fluorescence intensities of 4,6-TCD-GlcNAc/PAAm (gold) and 10,12-TCD-GlcNAc (blue) surfaces, without (e) and with (f) exposure to 5 μg/mL WGA. (g) Fluorescence intensities of sPDA/PAAm substrates exposed to specified concentrations of WGA; images in inset were acquired using a widefield epifluorescence microscope, thus intensities are not directly comparable to values in (e,f).

exposure). Recently, we have shown that differences in sPDA emission intensity relate to the efficiency of sPDA transfer from HOPG to PAAm.[56] Fluorescence emission intensity from TCD-GlcNAc monolayers prior to WGA exposure (Figure 3i, blue trace) is substantially lower than that for TCD-COOH (red), TCD-GlcA (gold), and TCD-OH (green) monolayers. Thus, the interfacial concentration of GlcNAc on PAAm is lower in comparison to other functional groups, by up to a factor of 10 in comparison with TCD-COOH and ∼5× in comparison with TCD-OH and TCD-GlcA.

To establish a ratio of WGA binding normalized for surface concentration of the functionalization moiety, the maximum emission intensity (I_{548}) of WGA-treated monolayers was divided by emission intensity at the PDA emission peak (I_{584}). Figure 3k shows WGA binding normalized for surface coverage, using this approach. The normalized WGA binding for the TCD-GlcNAc monolayer is 6 (TCD-OH) to 15 (TCD-COOH) times greater than other functional moieties, while binding to GlcA is similar to that observed for the OH and COOH patterns.

Conversely, the functionalized surfaces do not increase the adsorption of ConA (Figure 3l); exposure of fluorescence ConA to both TCD-GlcNAc-functionalized (red trace) and unfunctionalized (light red trace) PAAm produces similar fluorescence emissions, also comparable to that observed from WGA exposed to unfunctionalized PAAm (blue trace). Therefore, it appears that the interaction between WGA and the TCD-GlcNAc monolayer is highly selective.

To illustrate the capability to control lectin−carbohydrate interactions across geometrically controlled areas of the soft surface, we generated square patterns of TCD-GlcNAc sPDAs on HOPG by microcontact printing (μCP) (Figure 3m). After transfer to PAAm, the squares are visible in fluorescence images (Figure 3n; inset shows enhanced contrast); a larger area of the substrate is shown in this panel to facilitate visualization of the relatively faint pattern. Square patterns become clearly visible in both green and red channels of widefield epifluorescence images after exposure to WGA (Figure 4o).

Measurement of Surface Dissociation Constant (K_D). In principle, varying the length of the alkyl chain segment joining the carbohydrate to the sPDA backbone represents a means of controlling local concentration of carbohydrates along the stripe. In this context, short alkyl chain segments,

https://doi.org/10.1021/jacs.2c09937
J. Am. Chem. Soc. 2023, 145, 1668−1677

which decrease the volume available to each carbohydrate, would be expected to produce higher local concentration (effective molarity) of carbohydrates and potentially decrease K_D for a given surface coverage of the same carbohydrate.

To evaluate the effect of proximal chain length on GlcNAc spatial distribution, we created models of two isomers of TCD-GlcNAc with different proximal chain lengths: 4,6-TCD-GlcNAc (3-carbon proximal chain) and 10,12-TCD-GlcNAc (9-carbon proximal chain). Minimized molecular models of polymerized 4,6-TCD-GlcNAc and 10,12-TCD-GlcNAc monolayers on HOPG (Figure 4a,b) illustrate the potential for restrictions on the trajectories of GlcNAc headgroups based on the position of the PDA (highlighted in gold). The distance from the end of the GlcNAc to the PDA is ∼1.0 nm for 4,6-TCD-GlcNAc, increasing to ∼2.0 nm for 10,12-TCD-GlcNAc.

To better simulate the possible arrangement of GlcNAc when the PDA is suspended above a porous PAAm substrate, we performed sequential 1 ns molecular dynamics runs in explicit water, with the HOPG substrate removed from the model and the PDA backbone frozen (Figure 4c). This set of constraints was intended to mimic the periodic covalent linkage of the relatively stiff PDA (persistence length ∼16 nm) to the PAAm mesh, while allowing for the motion of pendant alkyl chain segments and headgroups. Models after dynamics illustrate that GlcNAc headgroups in the 4,6-TCD-GlcNAc layer are more tightly clustered, in comparison with those in models of 10,12-TCD-GlcNAc. Distances between pyranose rings along each PDA were evaluated, pooling 4 and 8 ns timepoints (Figure 4d), producing median values of 11.8 and 10.1 Å for C2−OH and C6−CO, respectively, for 4,6-TCD-GlcNAc. Equivalent calculations for 10,12-TCD-GlcNAc produced values of 13.8 and 12.5 Å, respectively. Although differences in median values are modest, the dotted gray tie line illustrates the distance between paired carbohydrate recognition sites on WGA (13 Å). Notably, due to a combination of the lower median values and tighter distribution of values for 4,6-TCD-GlcNAc, a much larger fraction of the distances between adjacent carbohydrates falls within this range (69 and 87%, respectively, for C2−OH and C6−CO in the 4,6-TCD-GlcNAc models, in comparison with values of 46 and 54% for the 10,12-TCD-GlcNAc models). The differences in lengths of the alkyl linkers connecting the PDA and carbohydrate headgroups for 4,6- and 10,12-TCD-GlcNAc may also contribute to differences in affinity in ways not directly related to local concentration effects, for instance by influencing the range of possible orientations for the carbohydrate headgroups.

To evaluate the effect of proximal chain length on GlcNAc−WGA binding avidity experimentally, we compared binding to 10,12-TCD-GlcNAc and 4,6-TCD-GlcNAc (see Scheme 1 for structure and synthesis). The transfer efficiency of both isomers to PAAm was similar within error, as measured by PDA fluorescence emission (Figure 4e). Following exposure to WGA (5 μg/mL), a large increase in fluorescence emission was observed for carbohydrate-functionalized surfaces, particularly near 584 nm, the emission maximum for the rhodamine label appended to WGA. Spectral distribution also changed to resemble that for the rhodamine label. Emission intensity from 4,6-TCD-GlcNAc + WGA monolayers is substantially greater than that from 10,12-TCD-GlcNAc + WGA monolayers at 5 μg/mL (Figure 4f), consistent with the prediction of increased binding to the more localized GlcNAc moieties.

Past studies have reported dissociation constants (K_D) for monovalent interactions between WGA and GlcNAc of 1.8 mM, with designed bivalent solution-phase ligands producing K_D values from 100 to 700 nM, depending on linker geometry, and tetravalent solution-phase ligands producing K_D values as low as 1−4 nM.[62] Studies of surface binding interactions between ConA and printed monolayers of mannosides comprising 1−9 units exhibited K_D values in the range of 80−90 nM for glycan densities sufficient to achieve multivalent binding (based on stochastic inter-glycan distance <6.5 nm) and >200 nM for lower surface concentrations of mannosides at which multivalent interactions should become statistically less likely.[28]

To evaluate whether WGA interaction with TCD-GlcNAc sPDAs are multivalent or monovalent, we exposed 10,12- and 4,6-TCD-GlcNAc/PAAm surfaces to increasing concentrations of WGA, maintaining the surface density of GlcNAc in the sPDA constant (Figure 4g). To calculate K_D for the WGA−GlcNAc surface interaction, we plotted the WGA concentration against the WGA emission intensity, and data were fit to a Langmuir isotherm,[28] which is widely used as a model for lectin−carbohydrate interfacial binding[26,28,32,63−66]

$$F = F_{max}[\mathrm{WGA}]/\{[\mathrm{WGA}] + K_D\}$$

where F_{max} is the maximum fluorescence intensity (an observable dependent on the GlcNAc−WGA interaction), [WGA] is the WGA concentration, and K_D is the equilibrium dissociation constant for surface GlcNAc and WGA. The emission intensity increases as [WGA] is increased from 0.5 to 5 μg/mL (Figure 4g) for both isomers, with greater emission from surfaces functionalized with 4,6-TCD-GlcNAc. 4,6-TCD-GlcNAc surfaces reach saturation at a lower WGA concentration (3 μg/mL) than 10,12-TCD-GlcNAc (7 μg/mL). As [WGA] is increased further, the emission intensity remains similar, typically associated with the saturation of GlcNAc ligands on the surface. For 4,6-TCD-GlcNAc, the intensity begins to increase again at 10−15 μg/mL. We observed similar behavior for 10,12-TCD-GlcNAc at concentrations higher than 15 μg/mL (see the Supporting Information). Previous studies have found similar binding curve shapes for multivalent systems in cases in which protein−protein interactions begin to occur at higher protein concentrations.[67] Since these features do not directly involve GlcNAc−WGA interactions, we excluded those data points from the binding curve (see detailed discussion in the Supporting Information). The value of K_D obtained from the WGA binding curve for 4,6-TCD-GlcNAc (10.1 ± 0.6 nM) is 3.6 times lower than that for 10,12-TCD-GlcNAc (36.1 ± 1.3 nM) and 1.8×10^5 times lower than previously reported K_D values for monomeric solution-phase GlcNAc−WGA interactions.[62] Values of K_D in the nM range are consistent with multivalent binding to the templated GlcNAc moieties, even when the overall surface coverage of GlcNAc is low.

CONCLUSIONS

Here, we have demonstrated that diacetylene amphiphiles with carbohydrate headgroups can be ordered on HOPG into striped phases with domain edge lengths from 100 nm to nearly 1 μm. Following photopolymerization, these unconventional surface-templated glycopolymers can be covalently transferred to the surfaces of hydrogels and used to generate selective multivalent binding to appropriate lectins.

https://doi.org/10.1021/jacs.2c09937
J. Am. Chem. Soc. 2023, 145, 1668−1677

Even at very low overall surface densities of carbohydrate, the local presentation is maintained by the surface-templated glycopolymer, resulting in K_D values (10−40 nM) that compare favorably with other surface binding strategies that require very high surface densities of carbohydrates.

We suggest that, in part, this may be due to high steric accessibility of the glycopolymers suspended over the porous hydrogel mesh. This combination of volume localization and steric accessibility is uniquely different from both conventional monolayer chemistries and stochastic hydrogel functionalization strategies (which place the majority of the appended functionalities in pores, where they are less accessible to large entities such as viruses and cells binding to the interface). Additionally, the relatively stiff PDA backbone (solution persistence length ∼16 nm)[44,45] points to the likely retention of an extended configuration of the polymers, somewhat analogous to extended conformations of mucins and other biological glycopolymers.

Such a capability has potential utility in the design of surfaces for studying glycan−lectin and other glycan−receptor interactions that depend on multivalency, particularly those in which interfacial mechanics may play a role. More broadly, the capability to pattern extended glycopolymers on soft materials, with both nanoscale and microscale features, may be useful in controlling interactions with larger functional structures such as cells and tissues, which commonly rely on multivalent interactions with carbohydrates in the extracellular matrix. In this regard, the capability to generate highly structured patterns of carbohydrates in the top few nanometers of a hydrogel surface may be of particular importance in designing mimics of structured interfacial environments common in the extracellular matrix. We note that, while in part the presentation of carbohydrates or other ligands may be altered by flexibility of the bulk gel (for instance, impacting alignment of adjacent polymers), the stiffness of the PDA is likely to, in part, offset the flexibility of the hydrogel mesh.

EXPERIMENTAL SECTION

See detailed Materials and Methods section in the Supporting Information.

ASSOCIATED CONTENT

Supporting Information

The Supporting Information is available free of charge at https://pubs.acs.org/doi/10.1021/jacs.2c09937.

Detailed materials and methods; large-scale AFM and SEM images comparing ordering of polymerizable amphiphiles on HOPG; large-scale fluorescence images illustrating sPDA monolayers transferred to PAAm; large-scale fluorescence images illustrating preferential binding of WGA with 10,12-TCD-GlcNAc/PAAm surfaces in comparison with other headgroup chemistries; cryoEM images of the unfunctionalized and functionalized PAAm hydrogel structure; polarized emission from transferred sPDA monolayers on PAAm hydrogels; additional discussion of WGA−WGA interactions observed at higher WGA concentrations; data analysis for fluorescence emission sampling; larger-scale SEM images illustrating the use of circular vacancies in sPDA monolayers as an internal standard for binding assays; larger images of output from molecular modeling; and ^{1}H and ^{13}C NMR spectra and HR mass spectra for all newly synthesized compounds (PDF)

AUTHOR INFORMATION

Corresponding Author

Shelley A. Claridge − *Department of Chemistry, Purdue University, West Lafayette, Indiana 47907, United States; Weldon School of Biomedical Engineering, Purdue University, West Lafayette, Indiana 47907, United States;* orcid.org/0000-0002-8599-0589; Phone: 765-494-6070; Email: claridge@purdue.edu

Authors

Anamika Singh − *Department of Chemistry, Purdue University, West Lafayette, Indiana 47907, United States*

Juan C. Arango − *Department of Chemistry, Purdue University, West Lafayette, Indiana 47907, United States*

Anni Shi − *Department of Chemistry, Purdue University, West Lafayette, Indiana 47907, United States*

Joseph B. d'Aliberti − *Department of Chemistry, Purdue University, West Lafayette, Indiana 47907, United States*

Complete contact information is available at: https://pubs.acs.org/10.1021/jacs.2c09937

Notes

The authors declare no competing financial interest.

ACKNOWLEDGMENTS

S.A.C. acknowledges support through a Showalter Research Trust grant and a Schmidt Science Polymaths Award. Instrumentation in the Purdue Imaging Facility was utilized for optical microscopy experiments.

REFERENCES

(1) Goldstein, I. J.; Hayes, C. E. The Lectins: Carbohydrate-Binding Proteins of Plants and Animals. *Adv. Carbohydr. Chem. Biochem.* **1978**, *35*, 127−340.

(2) Drickamer, K.; Taylor, M. E. Biology of Animal Lectins. *Annu. Rev. Cell Biol.* **1993**, *9*, 237−264.

(3) Koehler, M.; Delguste, M.; Sieben, C.; Gillet, L.; Alsteens, D. Initial Step of Virus Entry: Virion Binding to Cell-Surface Glycans. *Annu. Rev. Virol.* **2020**, *7*, 143−165.

(4) Syed, P.; Gidwani, K.; Kekki, H.; Leivo, J.; Pettersson, K.; Lamminmäki, U. Role of Lectin Microarrays in Cancer Diagnosis. *Proteomics* **2016**, *16*, 1257−1265.

(5) Purcell, S. C.; Godula, K. Synthetic Glycoscapes: Addressing the Structural and Functional Complexity of the Glycocalyx. *Biol. Pharm. Bull.* **2019**, *9*, 20180080.

(6) Honigfort, D. J.; Zhang, M. H.; Verespy, S.; Godula, K. Engineering of Spectator Glycocalyx Structures to Evaluate Molecular Interactions at Crowded Cellular Boundaries. *Faraday Discuss.* **2019**, *219*, 138−153.

(7) Kwan, C.-S.; Cerullo, A. R.; Braunschweig, A. B. Design and Synthesis of Mucin-Inspired Glycopolymers. *ChemPlusChem* **2020**, *85*, 2704−2721.

(8) Bertozzi, C. R.; Kiessling, L. L. Chemical Glycobiology. *Science* **2001**, *291*, 2357−2364.

(9) Kiessling, L. L.; Pohl, N. L. Strength in Numbers: Non-Natural Polyvalent Carbohydrate Derivatives. *Chem. Biol.* **1996**, *3*, 71−77.

(10) Prescher, J. A.; Bertozzi, C. R. Chemistry in Living Systems. *Nat. Chem. Biol.* **2005**, *1*, 13−21.

(11) Hirabayashi, J.; Arai, R. Lectin Engineering: The Possible and the Actual. *Biol. Pharm. Bull.* **2019**, *9*, 20180068.

(12) Tapia, B.; Yagudayeva, G.; Bravo, M. F.; Thakur, A. B.; Braunschweig, M.; Marianski, M. Binding of Synthetic Carbohydrate

Receptors to Enveloped Virus Glycans: Insights from Molecular Dynamics Simulations. *Carbohydr. Res.* **2022**, *518*, 108574.
(13) Nicolas, J.; Magli, S.; Rabbachin, L.; Sampaolesi, S.; Nicotra, F.; Russo, L. 3D Extracellular Matrix Mimics: Fundamental Concepts and Role of Materials Chemistry to Influence Stem Cell Fate. *Biomacromol* **2020**, *21*, 1968−1994.
(14) Rini, J. M. Lectin Structure. *Annu. Rev. Biophys. Biomol. Struct.* **1995**, *24*, 551−577.
(15) Han, X.; Zheng, Y.; Munro, C. J.; Ji, Y.; Braunschweig, A. B. Carbohydrate Nanotechnology: Hierarchical Assembly Using Nature's Other Information Carrying Biopolymers. *Curr. Opin. Biotechnol.* **2015**, *34*, 41−47.
(16) Wright, C. S.; Jaeger, J. Crystallographic Refinement and Structure Analysis of the Complex of Wheat Germ Agglutinin with a Bivalent Sialoglycopeptide from Glycophorin A. *J. Biol. Chem.* **1993**, *232*, 620−638.
(17) Kiessling, L. L.; Grim, J. C. Glycopolymer Probes of Signal Transduction. *Chem. Soc. Rev.* **2013**, *42*, 4476−4491.
(18) Hoshino, Y.; Nakamoto, M.; Miura, Y. Control of Protein-Binding Kinetics on Synthetic Polymer Nanoparticles by Tuning Flexibility and Inducing Conformation Changes of Polymer Chains. *J. Am. Chem. Soc.* **2012**, *134*, 15209−15212.
(19) Suzuki, Y. Sialobiology of Influenza: Molecular Mechanism of Host Range Variation of Influenza Viruses. *Biol. Pharm. Bull.* **2005**, *28*, 399−408.
(20) Harris, A.; Cardone, G.; Winkler, D. C.; Heymann, A. C.; Brecher, M.; White, J. M.; Steven, A. C. Influenza Virus Pleiomorphy Characterized by Cryoelectron Tomography. *Proc. Natl. Acad. Sci.* **2006**, *103*, 19123−19127.
(21) Overeem, N. J.; Vries, E.; Huskens, J. A Dynamic, Supramolecular View on the Multivalent Interaction between Influenza Virus and Host Cell. *Small* **2021**, *17*, 2007214.
(22) Weinbaum, S.; Tarbell, J. M.; Damiano, E. R. The Structure and Function of the Endothelial Glycocalyx Layer. *Annu. Rev. Biomed. Eng.* **2007**, *9*, 121−167.
(23) Di Maio, A.; Cioce, A.; Achilli, S.; Thépaut, M.; Vivès, C.; Fieschi, F.; Rojo, J.; Reichardt, N. C. Controlled Density Glycodendron Microarrays for Studying Carbohydrate-Lectin Interactions. *Org. Biomol. Chem.* **2021**, *19*, 7357−7362.
(24) Müller, C.; Despras, G.; Lindhorst, T. K. Organizing Multivalency in Carbohydrate Recognition. *Chem. Soc. Rev.* **2016**, *45*, 3275−3302.
(25) Lin, T. H.; Lin, C. H.; Liu, Y. J.; Huang, C. Y.; Lin, Y. C.; Wang, S. K. Controlling Ligand Spacing on Surface: Polyproline-Based Fluorous Microarray as a Tool in Spatial Specificity Analysis and Inhibitor Development for Carbohydrate Protein Interactions. *ACS Appl. Mater. Interfaces* **2017**, *9*, 41691−41699.
(26) Zhang, Y.; Li, Q.; Rodriguez, L. G.; Gildersleeve, J. C. An Array-Based Method to Identify Multivalent Inhibitors. *J. Am. Chem. Soc.* **2010**, *132*, 9653−9662.
(27) Fasting, C.; Schalley, C. A.; Weber, M.; Seitz, O.; Hecht, S.; Koksch, B.; Dernedde, J.; Graf, C.; Knapp, E.-W.; Haag, R. Multivalency as a Chemical Organization and Action Principle. *Angew. Chem., Int. Ed.* **2012**, *51*, 10472−10498.
(28) Liang, P. H.; Wang, S. K.; Wong, C. H. Quantitative Analysis of Carbohydrate-Protein Interactions Using Glycan Microarrays: Determination of Surface and Solution Dissociation Constants. *J. Am. Chem. Soc.* **2007**, *129*, 11177−11184.
(29) Park, S.; Gildersleeve, J. C.; Blixt, O.; Shin, I. Carbohydrate Microarrays. *Chem. Soc. Rev.* **2013**, *42*, 4310−4326.
(30) Gordus, A.; MacBeath, G. Circumventing the Problems Caused by Protein Diversity in Microarrays: Implications for Protein Interaction Networks. *J. Am. Chem. Soc.* **2006**, *128*, 13668−13669.
(31) Bian, S.; Zieba, S. B.; Morris, W.; Han, X.; Richter, D. C.; Brown, K. A.; Mirkin, C. A.; Braunschweig, A. B. Beam Pen Lithography as a New Tool for Spatially Controlled Photochemistry, and Its Utilization in the Synthesis of Multivalent Glycan Arrays. *Chem. Sci.* **2014**, *5*, 2023−2030.
(32) Oyelaran, O.; Gildersleeve, J. C. Glycan Arrays: Recent Advances and Future Challenges. *Curr. Opin. Chem. Biol.* **2009**, *13*, 406−413.
(33) Cohen, M.; Fisher, C. J.; Huang, M. L.; Lindsay, L. L.; Plancarte, M.; Boyce, W. M.; Godula, K.; Gagneux, P. Capture and Characterization of Influenza A Virus from Primary Samples Using Glycan Bead Arrays. *Virology* **2016**, *493*, 128−135.
(34) Hyun, J. Y.; Pai, J.; Shin, I. The Glycan Microarray Story from Construction to Applications. *Acc. Chem. Res.* **2017**, *50*, 1069−1078.
(35) Honigfort, D. J.; Altman, M. O.; Gagneux, P.; Godula, K. Glycocalyx Crowding with Mucin Mimetics Strengthens Binding of Soluble and Virus-Associated Lectins to Host Glycan Receptors. *Proc. Natl. Acad. Sci.* **2021**, *118*, No. e2107896118.
(36) Rabuka, D.; Forstner, M. B.; Groves, J. T.; Bertozzi, C. R. Noncovalent Cell Surface Engineering: Incorporation of Bioactive Synthetic Glycopolymers into Cellular Membranes. *J. Am. Chem. Soc.* **2008**, *130*, 5947−5953.
(37) Groszek, A. J. Preferential Adsorption of Long-Chain Normal Paraffins on MoS_2, WS_2 and Graphite from *n*-Heptane. *Nature* **1964**, *204*, 680.
(38) Rabe, J. P.; Buchholz, S. Commensurability and Mobility in 2-Dimensional Molecular Patterns on Graphite. *Science* **1991**, *253*, 424−427.
(39) Okawa, Y.; Akai-Kasaya, M.; Kuwahara, Y.; Mandal, S. K.; Aono, M. Controlled Chain Polymerisation and Chemical Soldering for Single-Molecule Electronics. *Nanoscale* **2012**, *4*, 3013−3028.
(40) Claridge, S. A. Standing, Lying, and Sitting: Translating Building Principles of the Cell Membrane to Synthetic 2D Material Interfaces. *Chem. Commun.* **2018**, *54*, 6681−6691.
(41) Bang, J. J.; Rupp, K. K.; Russell, S. R.; Choong, S. W.; Claridge, S. A. Sitting Phases of Polymerizable Amphiphiles for Controlled Functionalization of Layered Materials. *J. Am. Chem. Soc.* **2016**, *138*, 4448−4457.
(42) Shi, A.; Claridge, S. A. Lipids: An Atomic Toolkit for the Endless Frontier. *ACS Nano* **2021**, *15*, 15429−15445.
(43) Okawa, Y.; Aono, M. Linear Chain Polymerization Initiated by a Scanning Tunneling Microscope Tip at Designated Positions. *J. Chem. Phys.* **2001**, *115*, 2317−2322.
(44) Campbell, A. J.; Davies, C. K. L. Chain-Length Effects in Polydiacetylene Yellow Solutions. *Polymer* **1994**, *35*, 4787−4793.
(45) Rawiso, M.; Aime, J. P.; Fave, J. L.; Schott, M.; Müller, M. A.; Schmidt, M.; Baumgartl, H.; Wegner, G. Solutions of Polydiacetylenes in Good and Poor Solvents: A Light and Neutron Scattering Study. *J. Phys.* **1988**, *49*, 861−880.
(46) Hayes, T. R.; Lang, E. N.; Shi, A.; Claridge, S. A. Large-Scale Noncovalent Functionalization of 2D Materials through Thermally Controlled Rotary Langmuir-Schaefer Conversion. *Langmuir* **2020**, *36*, 10577−10586.
(47) Hayes, T. R.; Bang, J. J.; Davis, T. C.; Peterson, C. F.; McMillan, D. G.; Claridge, S. A. Multimicrometer Noncovalent Monolayer Domains on Layered Materials through Thermally Controlled Langmuir-Schaefer Conversion for Noncovalent 2D Functionalization. *ACS Appl. Mater. Interfaces* **2017**, *9*, 36409−36416.
(48) Davis, T. C.; Bechtold, J. O.; Hayes, T. R.; Villarreal, T. A.; Claridge, S. A. Hierarchically Patterned Striped Phases of Phospholipids: Toward Controlled Presentation of Carbohydrates. *Faraday Discuss.* **2019**, *219*, 229−243.
(49) Davis, T. C.; Bechtold, J. O.; Shi, A.; Lang, E. N.; Singh, A.; Claridge, S. A. One Nanometer Wide Functional Patterns with a Sub-10 Nanometer Pitch Transferred to an Amorphous Elastomeric Material. *ACS Nano* **2021**, *15*, 1426−1435.
(50) Shi, A.; Villarreal, T. A.; Singh, A.; Hayes, T. R.; Davis, T. C.; Brooks, J. T.; Claridge, S. A. Plenty of Room at the Top: A Multi-Scale Understanding of nm-Resolution Polymer Patterning on 2D Materials. *Angew. Chem., Int. Ed.* **2021**, *60*, 25436−25444.
(51) Bechtold, J. O.; Arango, J. C.; Shi, A.; Singh, A.; Claridge, S. A. Striped Poly(Diacetylene) Monolayers Control Adsorption of Polyelectrolytes and Proteins on 2D Materials and Elastomers. *ACS Appl. Nano Mater.* **2021**, *4*, 7037−7046.

https://doi.org/10.1021/jacs.2c09937
J. Am. Chem. Soc. 2023, 145, 1668−1677

(52) Villarreal, T. A.; Russell, S. R.; Bang, J. J.; Patterson, J. K.; Claridge, S. A. Modulating Wettability of Layered Materials by Controlling Ligand Polar Headgroup Dynamics. *J. Am. Chem. Soc.* **2017**, *139*, 11973−11979.
(53) Choong, S. W.; Russell, S. R.; Bang, J. J.; Patterson, J. K.; Claridge, S. A. Sitting Phase Monolayers of Polymerizable Phospholipids Create Dimensional, Molecular-Scale Wetting Control for Scalable Solution Based Patterning of Layered Materials. *ACS Appl. Mater. Interfaces* **2017**, *9*, 19326−19334.
(54) Porter, A. G.; Ouyang, T.; Hayes, T. R.; Biechele-Speziale, J.; Russell, S. R.; Claridge, S. A. 1-nm-Wide Hydrated Dipole Arrays Regulate AuNW Assembly on Striped Monolayers in Nonpolar Solvent. *Chem* **2019**, *5*, 2264−2275.
(55) Lang, E. N.; Porter, A. G.; Ouyang, T.; Shi, A.; Hayes, T. R.; Davis, T. C.; Claridge, S. A. Oleylamine Impurities Regulate Temperature-Dependent Hierarchical Assembly of Ultranarrow Gold Nanowires on Biotemplated Interfaces. *ACS Nano* **2021**, *15*, 10275−10285.
(56) Arango, J. C.; Williams, L. O.; Shi, A.; Singh, A.; Nava, E. K.; Fisher, R. V.; Garfield, J. A.; Claridge, S. A. Nanostructured Surface Functionalization of Polyacrylamide Hydrogels Below the Length Scale of Hydrogel Heterogeneity. *ACS Appl. Mater. Interfaces* **2022**, *14*, 43937−43945.
(57) Györgydeák, Z.; Hadady, Z.; Felföldi, N.; Krakomperger, A.; Nagy, V.; Tóth, M.; Brunyánszki, A.; Docsa, T.; Gergely, P.; Somsák, L. Synthesis of N-(Beta-D-Glucopyranosyl)- and N-(2-Acetamido-2-Deoxy-Beta-D-Glucopyranosyl) Amides as Inhibitors of Glycogen Phosphorylase. *Bioorg. Med. Chem.* **2004**, *12*, 4861−4870.
(58) Davis, T. C.; Bang, J. J.; Brooks, J. T.; McMillan, D. G.; Claridge, S. A. Hierarchical Noncovalent Functionalization of 2D Materials by Controlled Langmuir-Schaefer Conversion. *Langmuir* **2018**, *34*, 1353−1362.
(59) Hayes, T. R.; Bang, J. J.; Davis, T. C.; Peterson, C. F.; McMillan, D. G.; Claridge, S. A. Multimicrometer Noncovalent Monolayer Domains on Layered Materials through Thermally Controlled Langmuir-Schaefer Conversion for Noncovalent 2D Functionalization. *ACS Appl. Mater. Interfaces* **2017**, *9*, 36409−36416.
(60) Shi, A.; Singh, A.; Williams, L. O.; Arango, J. C.; Claridge, S. A. Nanometer-Scale Precision Polymer Patterning of PDMS: Multiscale Insights into Patterning Efficiency Using Alkyldiynamines. *ACS Appl. Mater. Interfaces* **2022**, *14*, 22634−22642.
(61) Lécuiller, R.; Berréhar, J.; Lapersonne-Meyer, C.; Schott, M. Dual Resonance Fluorescence of Polydiacetylene Chains Isolated in Their Crystalline Monomer Matrix. *Phys. Rev. Lett.* **1998**, *80*, 4068−4071.
(62) Rohse, P.; Weickert, S.; Drescher, M.; Wittmann, V. Precipitation-Free High-Affinity Multivalent Binding by Inline Lectin Ligands. *Chem. Sci.* **2020**, *11*, 5227−5237.
(63) Godula, K.; Bertozzi, C. R. Density Variant Glycan Microarray for Evaluating Cross-Linking of Mucin-Like Glycoconjugates by Lectins. *J. Am. Chem. Soc.* **2012**, *134*, 15732−15742.
(64) Shinohara, Y.; Sota, H.; Kim, F.; Shimizu, M.; Gotoh, M.; Tosu, M.; Hasegawa, Y. Use of a Biosensor Based on Surface Plasmon Resonance and Biotinyl Glycans for Analysis of Sugar Binding Specificities of Lectins. *J. Biochem.* **1995**, *117*, 1076.
(65) Branderhorst, H. M.; Ruijtenbeek, R.; Liskamp, R. M. J.; Pieters, R. J. Multivalent Carbohydrate Recognition on a Glycodendrimer-Functionalized Flow-through Chip. *ChemBioChem* **2008**, *9*, 1836−1844.
(66) Duverger, E.; Frison, N.; Roche, A. C.; Monsigny, M. Carbohydrate-Lectin Interactions Assessed by Surface Plasmon Resonance. *Biochimie* **2003**, *85*, 167−179.
(67) Mitchison, T. J. Beyond Langmuir: Surface-Bound Macromolecule Condensates. *Mol. Biol. Cell* **2020**, *31*, 2502−2508.

https://doi.org/10.1021/jacs.2c09937
J. Am. Chem. Soc. 2023, 145, 1668−1677